Iranian Journal of Geophysics, Vol 15 No 4, 2022, Page 53 – 69 (Research Article)
DOI: 10.30499/IJG.2021.260899.1307

Stress mapping, focal mechanism display and stress tensor inversion in Qeshm Island, Southern Iran

Shahrokh Pourbeyranvand [1*]

[1] *Assistant Professor, International Institute of Earthquake Engineering and Seismology, Tehran, Iran*

(Received: 07 December 2020, Accepted: 28 May 2021)

Abstract

Knowing about the stress field is essential to have insight into the seismotectonics and to understand the geodynamics of any study area. Stress tensor inversion is used for obtaining more precise stress information from cluster of earthquakes. Moreover, it is shown that the proper display of earthquake focal mechanism can help to get a better understanding of the seismotectonics of the region. In this study, the maximum horizontal stress directions in Qeshm Island, southern Iran, are extracted by using single earthquake focal mechanism. The Island is very important regarding its oil and gas reservoirs, still being explored, and planned industrial and business developments. Following previous studies in the region, there is an ambiguity in the main stress orientation in the area arising from the cross-cutting directions of the earthquake focal mechanism P axes. The stress tensor inversion of the focal mechanisms related to the 2005 earthquake aftershock sequence in Qeshm Island helped to resolve the observed ambiguity and revealed the correct maximum horizontal stress direction. The stress field is then mapped by implementing a new data visualization method. According to a circular color scale, this method is based on attributing RGB specific values to each rectangular grid cells. For a correct illustration of the directions with a color scale, the opposite directions (SHmax) should be of the same color, which necessitates introducing a new color wheel. The obtained anomaly in the stress direction coincides with the geological features and also InSAR results in the study area. These findings reveal the different stress field of the central parts of the Island, which is uplifted during the 2005 earthquake. Finally, it is proved that the 2005 earthquake and its aftershock sequence perturb the stress field in Qeshm Island.

Keywords: Stress direction, stress inversion, tectonic, data visualization, Qeshm Island, focal mechanism

[*] Corresponding author: beyranvand@iiees.ac.ir

1 Introduction

It is essential to know about the stress field to understand the motion on faults that cause earthquakes in Iran as one of the most seismically active countries on the earth. The Zagros, which is the most active seismotectonic province in Iran, extends from the Eastern Anatolian Fault in Turkey to the Makran Subduction in southern Iran. Due to its incredible complexity and importance of the convergence of the Arabian and Eurasian plates, many studies have been carried out in this region (e.g. Maggi et al., 2002; Regard et al., 2010; etc.). Since surface rupture with seismic activity is rare, most of the information available about active faults in this region is derived from earthquakes (Talebian and Jackson, 2004); however, it is usually difficult to attribute an earthquake to a specific fault due to the presence of a thick sedimentary cover that is about 10-14 km (Pirouz et al., 2017; McQuarrie, 2004). Seismicity in the Zagros is distinguished from other regions in Iran by a large number of small seismic events.

Stress state identification in Qeshm Island as a part of the Zagros Simply Folded Belt (Nissen et al., 2007) is necessary to study the deformation resulting from the oblique collision between the Eurasian and Arabian plates and to gain insight into the tectonics of this very important region. In Fig. 1, the earthquake focal mechanism data used in the present study is shown.

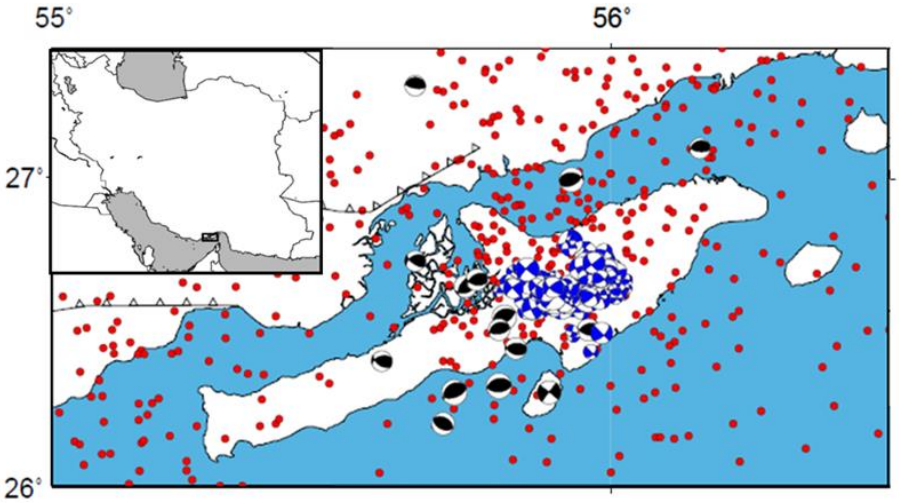

Fig 1. Map of the study area, including the focal mechanisms used in this study taken from different sources (explained in the text) and seismicity since 2006 (from IRSC). Inset map shows the location of the study area in southern Iran.

In the following sections, the method of extracting stress information from single focal mechanism data and also focal mechanism stress tensor inversion will be explained. Then, a new method of vector data visualization is proposed and the method is implemented for the tectonic stress derived from the methods mentioned above. Finally, the results are interpreted according to the geology of the area and new findings of this research are discussed.

2 Extraction of maximum horizontal stress directions from single focal mechanism data

Besides usual faulting regimes, including normal (NF), thrust or reverse (TF) and strike-slip faulting (SS), combinations of normal with strike-slip faulting or transtension (NS) and thrust with strike-slip faulting or transpression (TS) can also be introduced (Zoback, 1992). These stress regimes are shown in Fig. 2.

The plunges of P, B and T axes are

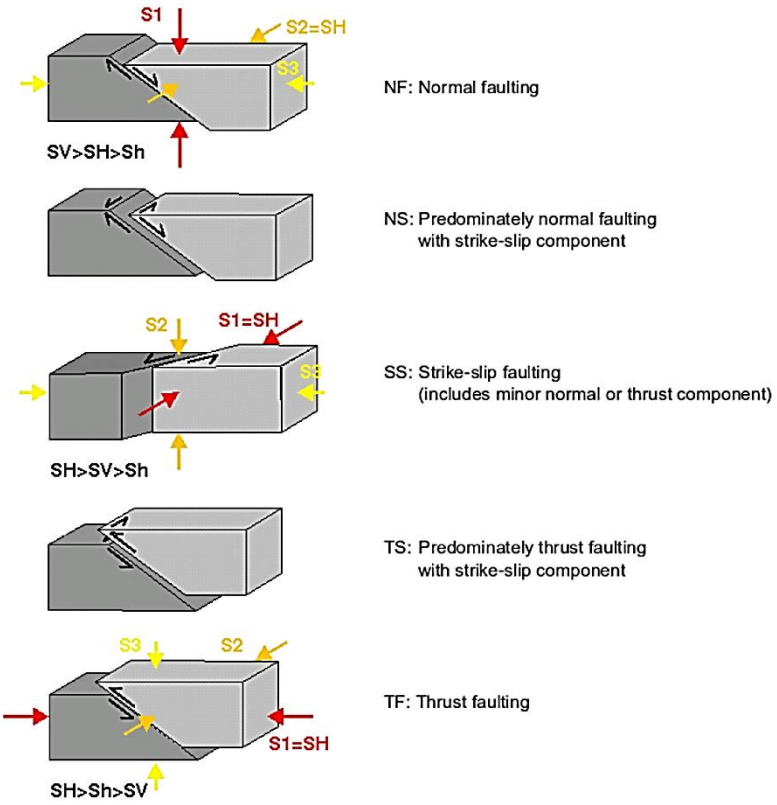

Fig 2. Classification of five different tectonic stress regimes and the related orientations of the principal stress axes (Heidbach et al., 2016).

P/S1-axis	B/S2- axis	T/S3- axis	Regime	S_H-azimuth
pl > 52		pl < 35	NF	azim. of B-axis
40 < pl < 52		pl < 20	NS	azim. of T-axis+90
pl < 40	pl > 45	pl < 20	SS	azim. of T-axis+90
pl < 20	pl > 45	pl < 40	SS	azim. of P-axis
pl < 20		40 < pl < 52	TS	azim. of P-axis
pl < 35		pl > 52	TF	azim. of P-axis

Table 1. Determination of σ1 directions from P, T and B axes orientations based on different tectonic stress regimes.

employed to determine the σ1 or maximum stress direction regarding the specific stress regime as shown in Table 1 (Zoback, 1992).

3 Earthquake focal mechanism data

The earthquake focal mechanism data of the study area were collected from different sources including teleseismic sources and published local networks data. These sources are the GCMT website (https://www.globalcmt.org/CMTsearch.html) (formerly abbreviated HRVD), the website of the Seismological Center of the Institute of Geophysics, University of Tehran (IRSC) (http://irsc.ut.ac.ir/bulletin.php/), the International Seismological Center (ISC) (http://www.isc.ac.uk/) website, the US National Earthquake Information Center website (NEIC) (https://earthquake.usgs.gov/earthquakes/search/) and the website of the Swiss Seismological Service ZUR_RMT (http://seismo.ethz.ch/en/home/). Furthermore, numerous articles were used to

complete the data set: Tatar et al. (2004), Gholamzadeh et al. (2009), Yaminifard et al. (2007), Yaminifard et al. (2012), Rezaei Nayeh (2011), Azadfar and Gheitanchi (2013) and Reza et al. (2014). The time frame of the focal mechanism data used in this study is from 1970 to 2020. Thus, the sources used to build the database of this study consist of teleseismic data (from international research centers including GCMT, USGS and ISC) and local data (including the focal mechanism data of IRSC and the local networks data of published scientific papers). Regarding the errors in the data, it should be mentioned that the uncertainty in the focal mechanism parameters is about 15 to 20 degrees. All of the earthquake foal mechanisms used in this study is present in Appendix 1.

The data are plotted in Fig. 3. This figure, a Kagan's triangular diagram, shows the nature of faulting for each event relative to three pure- normal, reverse and strike-slip mechanisms (Kagan, 2005). The events' depth and magnitude are also displayed by symbol color and size, respectively. It can be seen that most of the events, as expected, are reverse or strike-slip, which indicates the prevailing transpressional tectonic environment in the region.

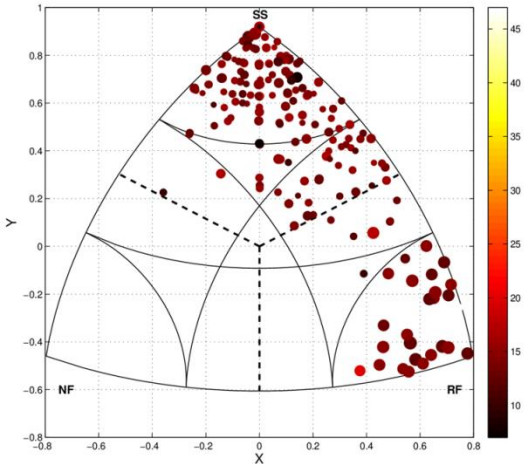

Fig 3. Kagan's triangular diagram showing the nature of faulting mechanisms all over the study area. The color scale on the right is used to determine the depth of events. The size of circles represents the magnitude of the events,

4 Visualization of the focal mechanism data

Recently, there have been some attempts to visualize the focal mechanism data in terms of a color scale (Hurd and Zoback, 2012). The nature of the focal mechanism data establishes some debates regarding the possibility and reliability of showing these data by a 2D colored grid. Such grids are suitable for displaying intrinsically continuous quantities such as topography, potential fields, etc.; however, earthquake faulting mechanisms can differ quite rapidly in short distances due to specific structural geology conditions. Although the visualization of these data is advantageous and gives a general overview of dominant faulting mechanisms of the study area, using false methods may be misleading and cause serious confusion. Since the nature of the phenomena under study is not continuous, as stated above, using interpolation may give completely wrong results in the display of the focal mechanism data.

Consider two points characterized by different reverse and normal mechanisms in a 2D plane map. If the color scale is designed so that these mechanisms are in the two extreme ends of a color pallet and the strike-slip places among them on the middle (Hurd and Zoback, 2012), inter-

polation rules out the grids in between to be strike-slip. This occurs even though there is no need to have a strike-slip faulting mechanism between two reverse and normal faulting in nature. In fact, there are several examples of collocated normal and reverse faults in subduction zones fore arcs and other geological environments (see e. g. Loveless, et al., 2010).

Dealing with these difficulties in displaying the earthquake focal mechanism data, it seems better to visualize the spatial variation of faulting mechanism without interpolation. For this purpose, the plunge angle of P, B and T axes of faulting mechanism are assigned to RGB components of color. There are two ways to do that. It is possible to plot the sized circles in the place of each focal mechanism location (Fig. 4a). The other way is to set the circles proportional to the magnitudes of the events (Fig. 4b). Comparing these two figures clearly shows how different data visualization methods may affect the understanding gained by looking at these figures. The importance of the magnitude of the events is evident in Fig. 4b. It describes that the dominant nature of faulting in the smaller local events is strike-slip (blue). In contrast, most of the large teleseismic events exhibit an almost pure reverse mechanism. A single comparatively small seismic event at the southern part of the Island shows a compound strike-slip-reverse mechanism. This event is expected owing to the existence of the observed transpressional environment in the study area.

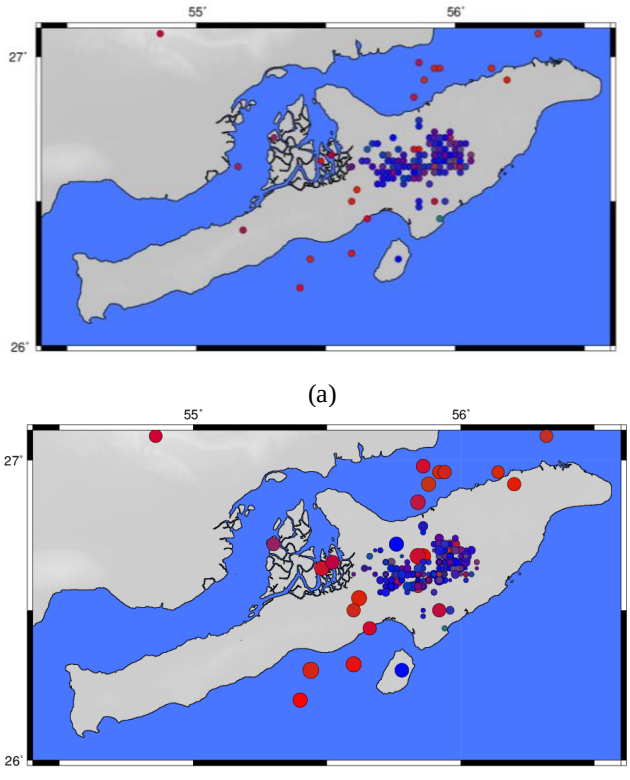

Fig 4. Focal mechanism display by plunge angles of T, P and B as RGB components (a) without magnitude, (b) with magnitude. The color of circles is red for pure reverse, green for pure normal and blue for pure strike-slip events.

5 The ambiguity about the stress state in Qeshm Island

As reflected in previous work in the area (Yaminifard et al., 2012), the stress state is ambiguous in Qeshm Island. They recognized that the earthquake focal mecha-

nism P axes show two different cross-cutting directions, which produces an ambiguity regarding the right maximum stress orientation in the study area. The rose diagram of the focal mechanism P axes in the study area (Fig. 5), including teleseismic and local events, shows three main directions as candidates for the maximum horizontal stress directions in Qeshm Island. The solution to this problem can be achieved by stress inversion of the earthquake focal mechanism data.

Here, there are arguments in using aftershock sequence for stress tensor inversion purposes since they do not sample different parts of the data space. The main claim is that all of the similar data available in an aftershock sequence may represent only one data and should not be used in the stress inversion procedure (Martínez-Garzón et al, 2016). But in the current circumstance, when there is a debate on the stress state based on the focal mechanism P axes data on the one hand, and a severe shortage in focal mechanism data on the other hand, the aftershock sequence should be used certainly to resolve the above mentioned ambiguity.

It is worthy to remind that the P axis of the earthquake focal mechanism is not always equivalent or even an indicator of the σ_1 or the maximum horizontal stress direction. The choice of an appropriate axis to gain information about the stress state depends on the earthquake mechanism, as described in Table 1. But here, since all of the events in Qeshm Island are reverse or strike-slip, their maximum stress direction can be approximated by the P axis according to Table 1. Thus, it is reasonable to consider the various P axis main orientations as the ambiguity in the tectonic stress field.

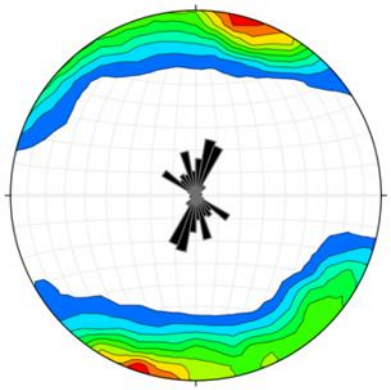

Fig 5. Rose diagram of earthquake focal mechanism P axes in Qeshm Island.

Afterward, the stress inversions using 183 local earthquake focal mechanisms from YaminiFard et al. (2012) are performed. The inversion results show that the orientation of σ_1 clearly is north-northwest, as it will be seen later in this research.

It is notable that the seismicity of Qeshm Island is totally changed after the 2005 earthquake (Fig. 6). Thus, in the future parts of this paper, the investigations on the earthquakes in the area will be devided up into two different parts: before and after 2005 earthquake.

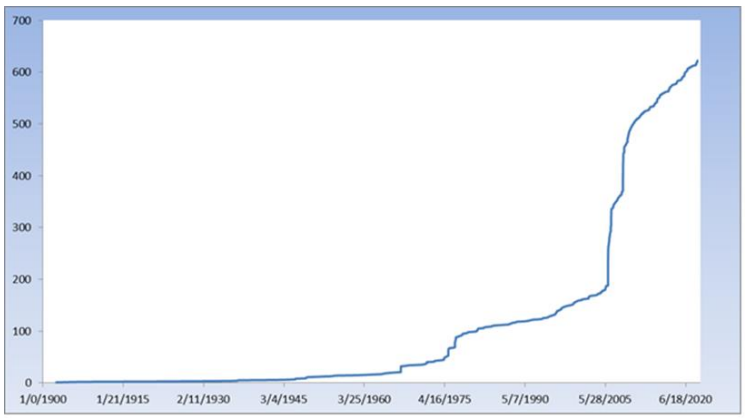

Fig 6. The cumulative number of seismic events in Qeshm Island since 1900 up to 2020 (from IIEES catalog), showing a sudden grow up following the 2005 earthquake.

6 Focal mechanism stress tensor inversion method

The stress tensor inversion is based on assumptions such as taking the slickensides parallel to the maximum resolved shear stress on the fault surface and homogeneity of the stress field in the study area (Wallace, 1951; Bott, 1959). The procedure was applied to geological fault slip data at the beginning (e.g. Angelier, 1984; Michael, 1984; Gephart and Forsyth, 1984) and then extended to earthquake focal mechanisms. The transformation between the two above schemes is easy, except for choosing the fault plane known in fault slip analysis and should be estimated using extra information and special methods in focal mechanism stress inversion.

The implemented method (Lund and Slunga, 1999), based on Gephart and Forsyth (1984), searches the principal stresses and relative size of the intermediate principal stress ellipsoid defined as $R = (\sigma_1 - \sigma_2)/(\sigma_1 - \sigma_3)$ through all directions and a range from zero to one, respectively. In the slip angle approach, the angle in the fault plane between the modeled maximum shear stress direction and the observed slip direction is minimized through the inversion. In the instability approach, considering the friction coefficient of rock layers, the nodal plane, which is more prone to failure, is identified; thus, this latter method is more physically based, and its results are expected to be more realistic (Lund and Slunga, 1999).

7 Stress inversion of earthquake focal mechanisms in Qeshm Island

In Fig. 7, using two different approaches, slip angle and instability, the stress inversion results are shown. The approaches deal with selecting the fault plane from the nodal planes. The slip angle method which is a mathematical method, only considers the angular difference or misfit angle between calculated and observed slip direction. The instability method has a physical basis and is expected to give more realistic results. It calculates which nodal plane is more instable according to Mohr-Coulomb criteria, friction coefficient and other parameters defined for each study.

The above-discussed ambiguity in the earthquake focal mechanism P axes is evident in these two different stress inversion results. The data used in this inversion consisted of 16 teleseismic earthquake focal mechanisms, obtained through international research centers, mentioned in the focal mechanism data section. The inversion quality is reflected in the confidence regions of the principal stress axes on the stereonets. The smaller the area of the confidence regions, the higher the quality of the inversion. By looking at the stereonets, it is clear that there is a high level of uncertainty in determining the σ_1 in both approaches. The optimum orientations of the mentioned stress axes are NE and NW that obviously defer by an angle of about 45 degrees. This angle of discrepancy is the same as the difference observed between the main trends of the P axes of main earthquakes (Yamini Fard, et al., 2012).

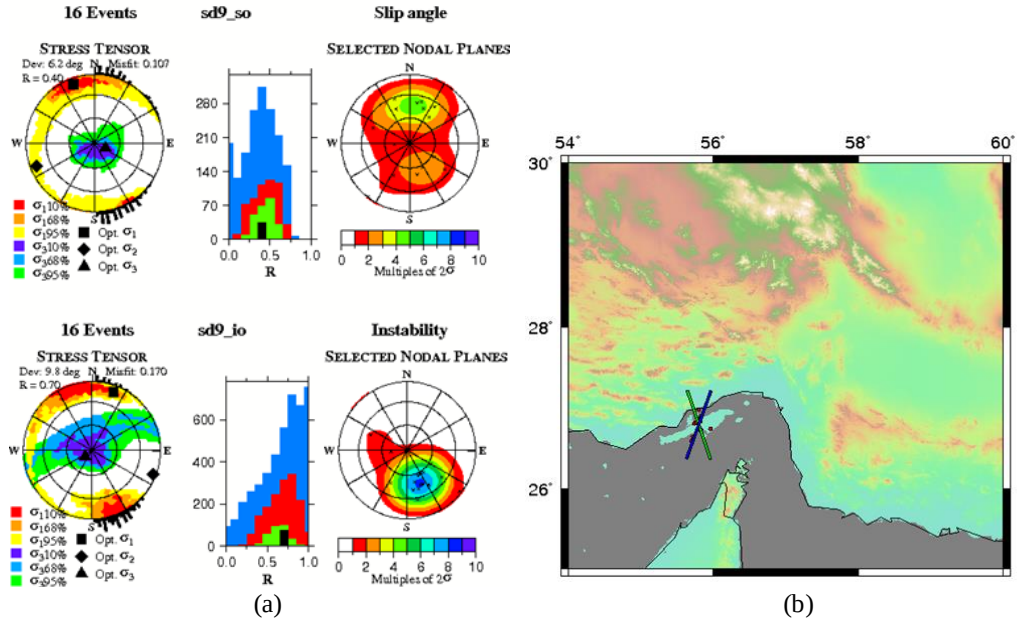

Fig 7. (a) Stress inversion results derived from teleseismic earthquake focal mechanisms. (b) Map of SHmax directions obtained by two inversion methods of misfit angle and instability.

After including the aftershock sequence in the inversion procedure, the confidence regions are shown to be smaller. Hence, the quality of the inversions and consequently the reliability of the answers are higher. The focal mechanism of events recorded at the local seismic network operated after the 2005 Qeshm earthquake are inverted for the stress state (Fig. 8). It is clear that both methods provide the same direction of σ_1, and the discussed ambiguity is resolved. Ultimately, the SHmax direction is proved to be NW in Qeshm Island.

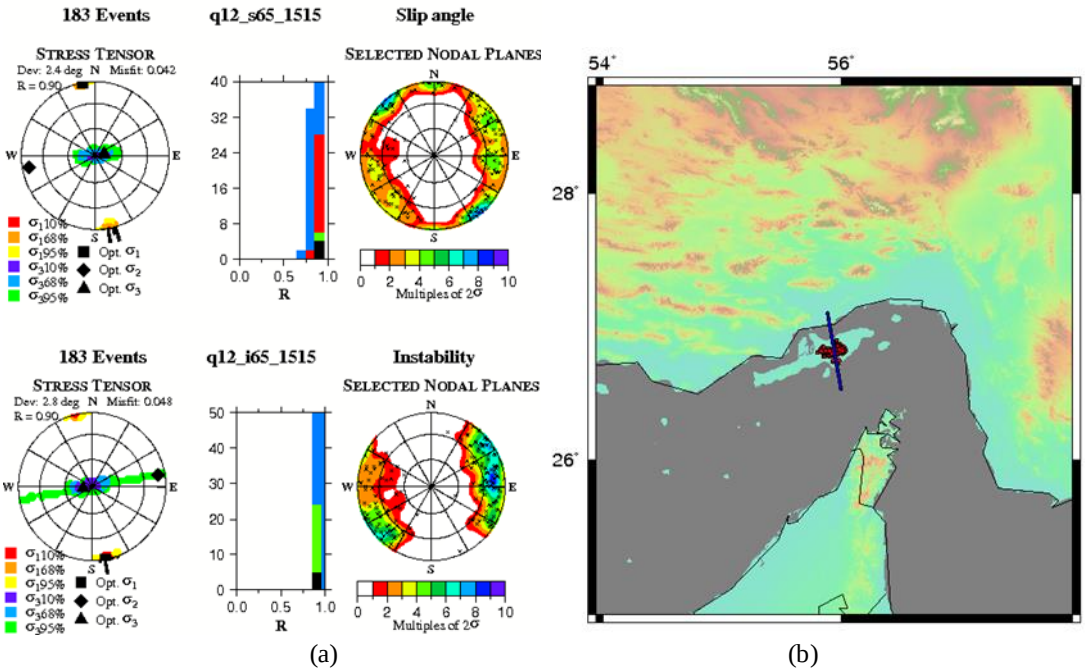

Fig 8. (a) Stress inversion results derived from local earthquake focal mechanisms. (b) Map of SHmax directions obtained by two inversion methods of misfit angle and instability.

8 A new method in visualizing the stress direction data

The first solution to solve this problem, i.e., showing the direction by a color scale, is to assign RGB combinations in different directions. However, if you increase one, two or three values of RGB, the result is not satisfying because the color contrast between 0 and 359, which should be very little, will be the highest value, and that is apparently false. On the other hand, the color of each direction and its neighbor, which is the same angle +180 degrees, should be the same. This requires a new circular color scale with central symmetry and makes the problem a little bit more challenging and totally differentiates the problem and solution from the previously known color wheel (Shevell, 2003). For the proposed new method, the circle is as Fig. 9.

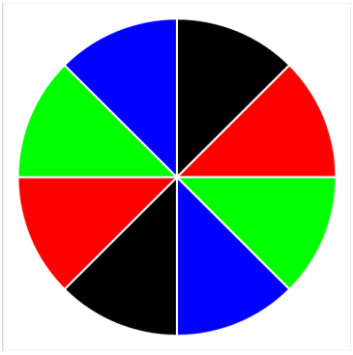

Fig 9. The proposed color wheel.

The RGB values for this new circle are shown in Table 2.

To show the pattern of increase and decrease in RGB values, the diagram in Fig. 10 will be obtained. Fig. 10a shows the three Red-Green-Blue value variations and Fig. 10b shows the combination of the charts related to the proposed color circle.

Consequently, we can further divide the whole circle and obtained finer patterns for the new color wheel. Indeed, by this act, the resolution of the color pallet used for vector data visualization purposes will be made higher. Table 3 shows the RGB color values.

Table 2. RGB values for the proposed color circle.

	R	G	B
0	0	0	0
45	256	0	0
90	0	256	0
135	0	0	256
180	0	0	0
225	256	0	0
270	0	256	0
315	0	0	256
360	0	0	0

The related RGB color patterns can be found in Fig. 11 for 8, 16 and 32 sectors for the proposed color circle.

As can be seen in Fig. 11, the pattern remains constant for each color circle type. Only the number of the dots in the edges are increased, which means higher accuracy or resolution of the plots using a higher number of sectors. In Fig. 12, the resulted color circles are shown.

Thus, by continuing and further dividing the circle into more sectors, we can assign more colors to angle intervals by creating high-resolution color pallets to map tools like GMT.

The CPT file for the proposed color circle can be 2048 line at its highest. Therefore, the highest resolution of the CPT files within this new method is achieved, but the CPT files with 128 and 512 lines give the same image for the current dataset. This happens because the resolution of the data is insufficient to employ the full range of the proposed visualization capacity of methods. We will refer to the CPT file related to the proposed color circle as dir2048.CPT file (Table 3).

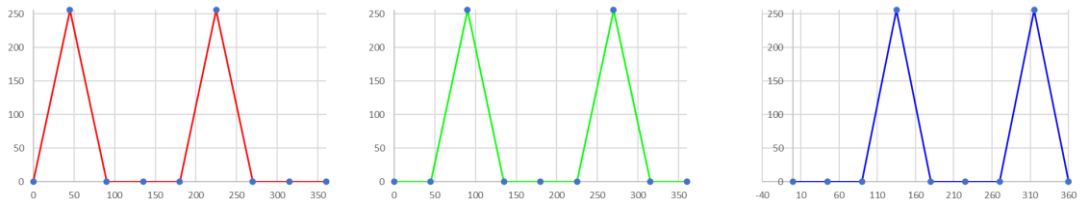

(a)

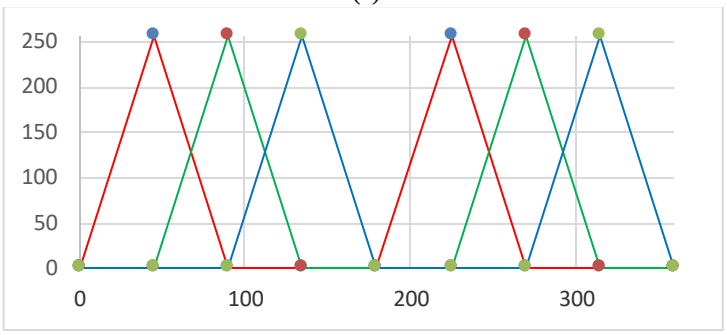

(b)

Fig 10. (a) Diagrams showing the individual variation of RGB values. (b) The combination of the charts related to the proposed color circle.

	R	G	B
0	0	0	0
45	256	0	0
90	0	256	0
135	0	0	256
180	0	0	0
225	256	0	0
270	0	256	0
315	0	0	256
360	0	0	0

	R	G	B
0	0	0	0
22.5	128	0	0
45	256	0	0
67.5	128	128	0
90	0	256	0
112.5	0	128	128
135	0	0	256
157.5	0	0	128
180	0	0	0
202.5	128	0	0
225	256	0	0
247.5	128	128	0
270	0	256	0
292.5	0	128	128
315	0	0	256
337.5	0	0	128
360	0	0	0

	R	G	B
0	0	0	0
11.25	64	0	0
22.5	128	0	0
33.75	192	0	0
45	256	0	0
56.25	192	64	0
67.5	128	128	0
78.75	64	192	0
90	0	256	0
101.25	0	192	64
112.5	0	128	128
123.75	0	64	192
135	0	0	256
146.25	0	0	192
157.5	0	0	128
168.75	0	0	64
180	0	0	0
191.25	64	0	0
202.5	128	0	0
213.75	192	0	0
225	256	0	0
236.25	192	64	0
247.5	128	128	0
258.75	64	192	0
270	0	256	0
281.25	0	192	64
292.5	0	128	128
303.75	0	64	192
315	0	0	256
326.25	0	0	192
337.5	0	0	128
348.75	0	0	64
360	0	0	0

Table 3. RGB values for the proposed color circle with 8, 16 and 32 sectors.

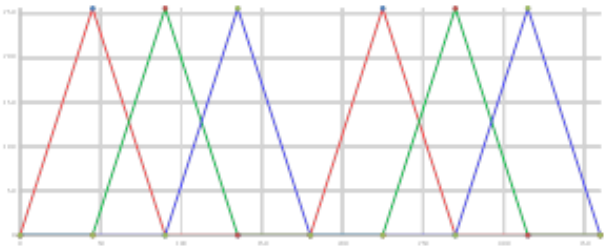

(a)

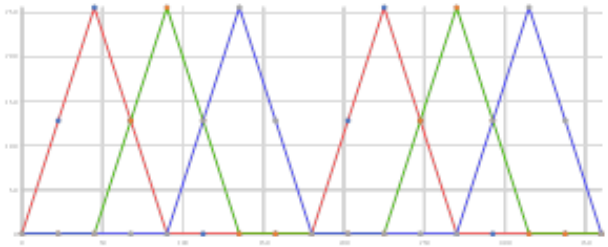

(b)

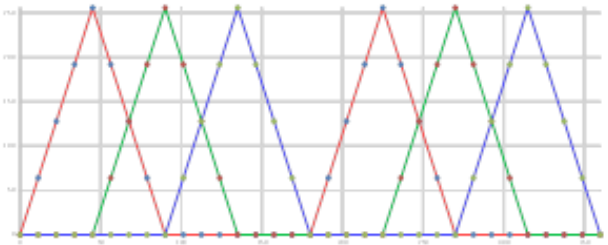

(c)

Fig 11. Diagrams showing the RGB combinations for the proposed color circle with (a) 8 (b) 16 (c) 32 sectors.

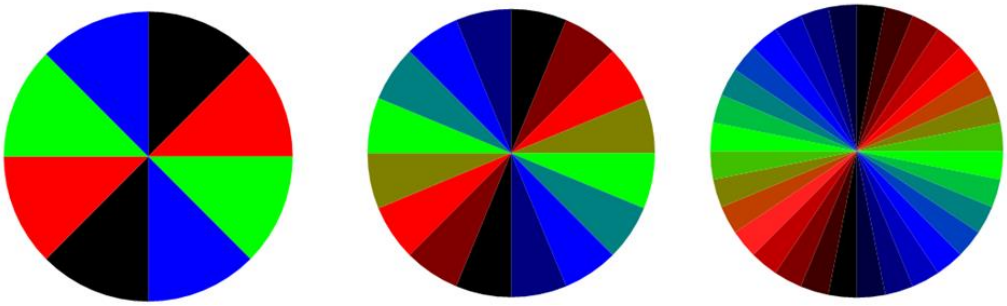

Fig 12. The proposed color circle with (a) 8 (b) 16 (c) 32 sectors.

It should be noted that the circular color scale can not only visualize the direction of vector data but also can show the magnitude of the vectors by subdividing the sectors and changing the saturation of the colors in a way that it can represent the magnitude changes. This method is not implemented in the present study, because our case study, which is about the stress direction, does not contain magnitude data.

9 Results and discussion

The proposed data visualization method is implemented for stress data available in the study area. The color pallet values are assigned to each cell and interpolation is used when needed. In other words, where the cells do not contain any data, appropriate colors by interpolation fill the cells. The proper use of GMT commands does this. By applying the method and using the dir2048.CPT file, Fig. 12 was obtained.

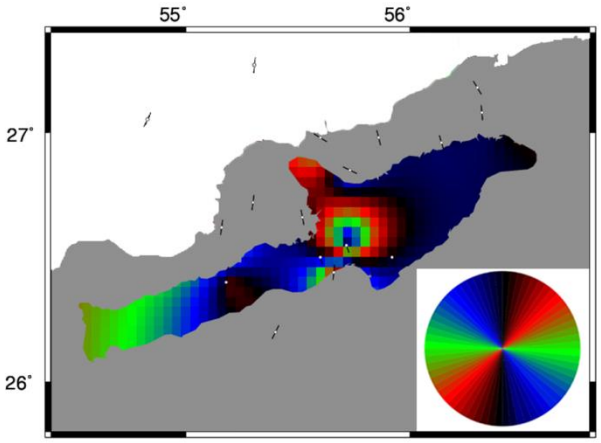

Fig 13. Stress mapping with the proposed circular color scale in the lower right corner using the stress information from teleseismic earthquake focal mechanisms.

Fig. 13 contains an unseen anomaly in the stress directions associated with teleseismic earthquakes and provides the first real color scaled stress maps in the study area. There is specific evidence of a correlation between the obtained anomaly in stress principal directions in Fig. 13 and the real geological situation on the ground. As shown in Fig. 14, InSAR processed satellite interferograms display the concentration of the displacement in the area, which exactly coincides with the anomaly in Fig. 14. From many works on the co-seismic interferometry of Qeshm 2005 earthquake, two outcomes are represented as examples to show a high degree of the claimed correlation (Amighpey et al., 2015; Nissen et al., 2007).

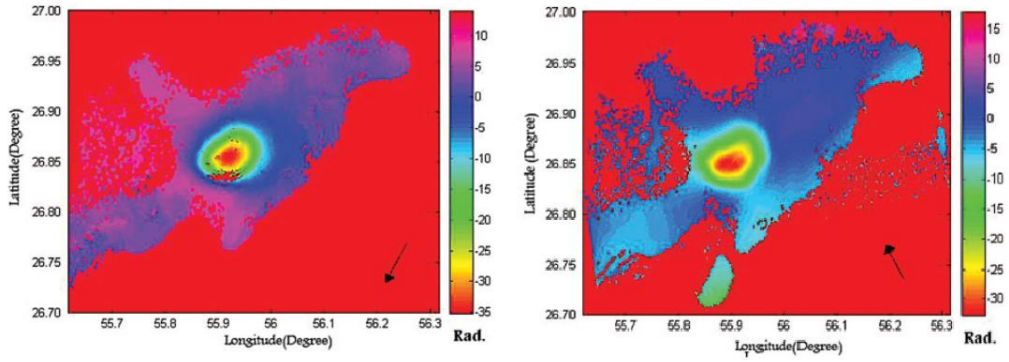

(a)

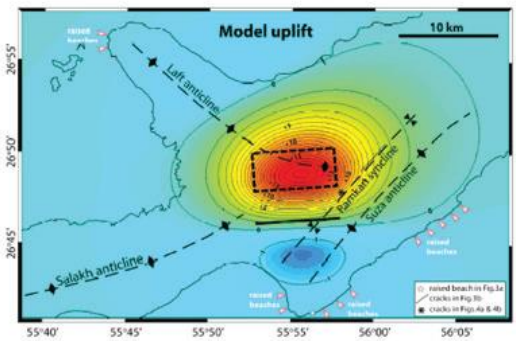

(b)

Fig 14. InSAR processed images of Qeshm Island after the 2005 earthquake showing the uplifted region associated with co-seismic deformation of the 2005 earthquake. (a) from Amighpey et al. (2015) and (b) from Nissen et al. (2007).

There are several syncline and anticlines in the Island (Fig. 15). The salt tectonic activitiy is a possible cause for the uplifts associated with the 2005 Qeshm earthquake (Amighpey et al., 2015). It can also be responsible for the anomalous co-seismic deformation and the observed anomaly in the stress directions in Qeshm Island. There are numerous examples of the influence of salt tectonics on faulting geometry and mechanism all over the world (Koyi and Petersen, 1993; Alsop et al., 1996; Stewart, et al., 1996; Harding and Huuse, 2015; Jackson and Lewis, 2015).

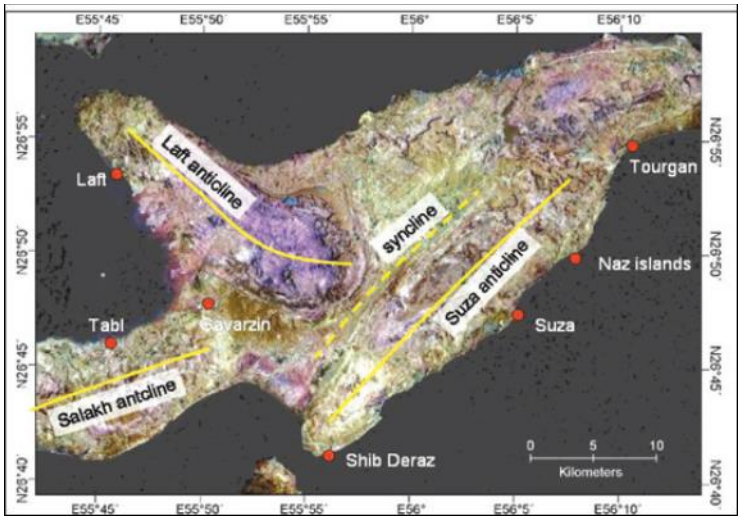

Fig 15. Geological explanation of the structural features visible on the satellite imagery of Qeshm Island. The salt dome in the center of the Island corresponds with the uplifted area shown in InSAR results (Amighpey et al., 2015).

By applying the method on the after-shock sequence focal mechanisms, a view of post-earthquake stress field is obtained (Fig. 16). The mainshock depth and mechanism differ from the depth and mechanism of aftershocks. Thus, using the present method of stress mapping, results in a map with a different view of the study area compared to Fig. 13, which is under the influence of the mainshock.

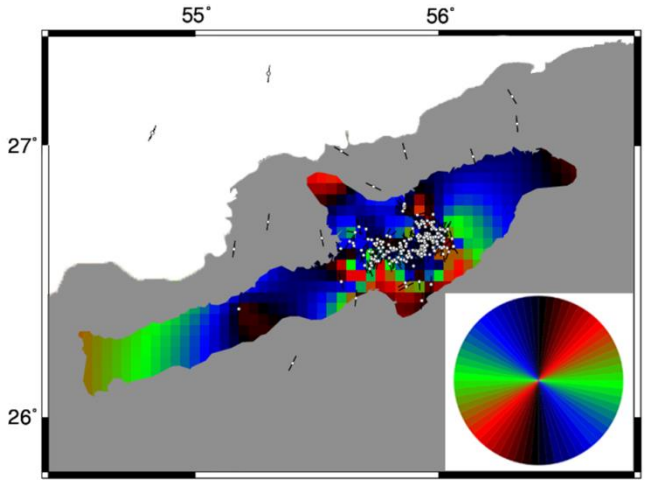

Fig 16. Stress mapping with the proposed circular color scale in the lower right corner using the stress information from 2005 aftershock sequence earthquake focal mechanism.

Focal mechanisms of the earthquakes considered as the aftershock sequence of the 2005 earthquake are strike-slip, different from the mainshock with the reverse mechanism. The mainshock occurred at shallower depth compared to the aftershocks and separated, deeper aftershocks followed it. Different deformation mechanisms in the sedimentary cover and the basement in Qeshm Island are evidenced (Yamini Fard et al., 2012). In fact, the occurrence of the reverse mainshock in the sedimentary layer has triggered a series of strike-slip events in the basement (Yamini Fard et al., 2012).

Taking the above fact into consideration, it is obvious that the stress field obtained from the shallow events related to the sedimentary cover is different from that of the deeper events belonging to the crystalline basement (Yamini Fard et al., 2012). We should note that seismicity within the sedimentary cover is well explained in the technical literature related to the seismotectonic setting of the area. The Paleozoic so-called competent layer is highly stiffened so that it can form asperities to originate seismic events (Nissen et al., 2011). The earthquakes are observed in the depth range equal to the thickness of sedimentary cover, which can be up to 14 km in the area (Pirouz et al., 2017); then, according to Figs. 12 and 15, there is a clear difference in the stress field between shallow and deep seismogenic zones. The observed perturbation in the stress field results from the occurrence of 2005 earthquake and its aftershock sequence in Qeshm Island.

The results of the present study alongside many other articles (e.g. Hensch et al., 2015; Wang et al. 2015; Sakaguchi and Yokoyama, 2017; Shebalin and Narteau, 2017; etc.) show that the stress field can be perturbed as a result of major earthquakes. Not. only the orientation of the principal stress axes, but also their magnitudes can show variations before and after the occurrence of the events. Thus, each earthquake can affect the surrounding stress field on its own. The larger the energy release, the greater the perturbation of the stress field; therefore, the stress field before and after the 2005 event in Qeshm Island is different. Stress field mapping by suggested data visualization method clearly shows how much the stress field is different before and after the mainshock and aftershock sequence.

It is confirmed by this study that the stress field deduced from deeper strike-slip faulting mechanisms related to aftershock sequence of 2005 earthquake in Qeshm Island recorded by a local network, is different from the stress orientation obtained from the mainshock and other major recorded teleseismic earthquakes in the area. This happened because the sedimentary cover and the basement do not accommodate the shortening in the same way and deformation partitioning happens due to the presence of pre-existing fault and fractures in the area. Deformation partitioning has been reported in several other case studies throughout the Zagros, with variable mechanisms including strike-slip and thrust motions because of oblique convergence between Arabia and Euraisa (Yaminifard et al., 2007).

10 Conclusion

This research showed that the proper display of earthquake focal mechanism could help to have a better insight into the seismotectonics of Qeshm Island. Focal mechanism stress tensor inversion of the 2005 earthquake aftershock sequence helped resolve the ambiguity in maximum horizontal stress direction and prove the SHmax to be NNW. The obtained anomaly in the stress direction is in agreement with the geological features and also InSAR results in the study area. By implementing a new data visualization method, it is shown that the stress field of the central parts of the Island,

which is uplifted during the 2005 earthquake, is different from the surrounding area, similar to the concentrated displacement field observed in InSAR images. The obtained stress maps proved the 2005 earthquake and its aftershock sequence perturbed the stress field in Qeshm Island

References

Alsop, G. I., Blundell, D. J., and Davison, I., 1996, Salt Tectonics: Geological Society of London.

Amighpey, M., Vosoughi, B., and Motagh, M., 2015, Assesment of source parameters of Qeshm 2005 earthquake based on InSAR observation inversion using genetic algorithm: Scientific Quarterly Journal of Geosciences, **24**(95), 343-350 (in Persian).

Angelier, J., 1984, Tectonic analysis of fault slip data sets: J. Geophys. Res., **89**, 5838-5848.

Azadfar, M., and Gheitanchi, M., 2013, Identifying causative fault of 11th May 2013 Goharan earthquake using reloction of aftershocks and focal mechanism: Iranian Journal of Geophysics, **9**(4), 54-67 (in Persian).

Bott, M. H. P., 1959, The mechanics of oblique-slip faulting: Geological Magazine, **96**, 109-117.

Gephart, J. W., and Fortyth, D. W., 1984, An improved method for determining the regional stress tensor using earthquake focal mechanism data: Application to the San Fernando earthquake sequence: Journal of Geophysical Research, **89**, 9305-9320.

Gholamzadeh, A., Yamini-Fard, F., Hessami, K., and Tatar, M., 2009. The February 28, 2006, Tiab earthquake, Mw 6.0: Implications for tectonics of the transition between the Zagros continental collision and the Makran subduction zone: Journal of Geodynamics, **47**, 280–287.

Harding, R., and Huuse, M., 2015, Salt on the move: Multi stage evolution of Salt diapirs in the Netherlands North Sea: Marine and Petroleum Geology, **61**, 39-55, doi:10.1016/j.marpetgeo.2014.12.003.

Heidbach, O., Rajabi, M., Cui, X., Fuchs, K., Müller, B., Reinecker, J., Reiter, K., Tingay, M., Wenzel, F., Xie, F., Ziegler, M. O., Zoback, M. L., and Zoback, M. D., 2018, The world stress map database release 2016: Crustal stress pattern across scales: Tectonophysics, **744**, 484-498, doi org/10.1016/j.tecto.2018.07.007.

Hensch, M., Lund, B., Árnadóttir, T., and Brandsdóttir, B., 2015, Temporal stress changes associated with the 2008 May 29 Mw 6 earthquake doublet in the western South Iceland seismic zone: Geophysical Journal International, **204**(1), 544-554, doi:10.1093/gji/ggv465.

Hurd, O., and Zoback, M. D., 2012, Intraplate earthquakes, regional stress and fault mechanics in the Central and Eastern U.S. and Southeastern Canada: Tectonophysics, **581**, 182–192.

Jackson, C. A., and Lewis, M. M., 2015, Structural style and evolution of a salt-influenced rift basin margin; the impact of variations in salt composition and the role of polyphase extension: Basin Research, **28**(1), 81-102, doi:10.1111/bre.12099.

Kagan, Y. Y., 2005, Double-couple earthquake focal mechanism: random rotation and display: Geophys. J. I., **163**(3), 1065–1072, doi.org/10.1111/j.1365-246X.2005.02781.x.

Koyi, H., and Petersen, K., 1993, Influence of basement faults on the development of salt structures in the Danish Basin: Marine and Petroleum Geology, **10**(2), 82-94, doi:10.1016/0264-8172(93)90015-k.

Loveless, J. P., Allmendinger, R. W., Pritchard, M. E., and González,G., 2010, Normal and reverse faulting driven by the subduction zone earth-

quake cycle in the northern Chilean forearc: Tectonics, **29**(2), https://doi.org/10.1029/2009tc002465.

Lund, B., and Slunga, R., 1999, Stress tensor inversion using detailed microearthquake information and stability constraints: Application to Olfusin southwest Iceland: J. Geophys. Res., **104**(B7), 14947-14964.

Maggi, A., Priestley, K., and Jackson, J., 2002, Focal depths of moderate to large earthquakes in Iran: Journal of Seismology and Earthquake Engineering, **4**(2&3), 1-10.

McQuarrie, N., 2004, Crustal scale geometry of the Zagros fold-thrust belt, Iran: Journal of Structural Geology, **26**, 519–535.

Martínez-Garzón, P., Ben-Zion, Y., Abolfathian, N., Kwiatek, G., and Bohnhoff, M., 2016, A refined methodology for stress inversions of earthquake focal mechanisms: J. . Geophys. Res., Solid Earth, **121**(12), 8666-8687, doi:10.1002/2016jb013493.

Michael, A. J., 1984, Determination of stress from slip data: faults and folds: J. . Geophys. Res., **89**(B13), 11517–11526.

Nissen, E., Ghorashi, M., Jackson, J., Parsons, B., and Talebian, M., 2007, The 2005 Qeshm Island earthquake (Iran)- a link between buried reverse faulting and surface folding in the Zagros simply folded belt?: Geophysical Journal International, **171**(1), 326-338, doi 10.1111/j.1365-246x.2007.03514.x.

Nissen, E., Tatar, M., Jackson, J. A., and Allen, M. B., 2011, New views on earthquake faulting in the Zagros fold-and-thrust belt of Iran: Geophys. J. I., doi: 10.1111/j.1365-246X.2011.05119.x.

Pirouz, M., Avouac, J. P., Gualandi, A., Hassanzadeh, J., and Sternai, P., 2017, Flexural bending of the Zagros foreland basin: Geophys. J. I., **210**(3), 1659–1680, doi: 10.1093/gji/ggx252.

Regard, V., Hatzfeld, D., Molinaro, M., Aubourg, C., Bayer, R., Bellier, O., and Abbassi, M. R., 2010, The transition between Makran subduction and the Zagros collision: Recent advances in its structure and active deformation: Geological Society, London, Special Publications, **330**(1), 43-64, doi:10.1144/sp330.4.

Reza, M., Abbasi, M. R., Javan Doloei, G., and Sadidkhuy, A., 2014, Identifying fault of Mohammad Abad Rigan 20/12/2010 earthquake and its focal mechanism using aftershock analyses: Iranian Journal of Geophysics, **8**(1), 59-70 (in Persian).

Rezaei Nayeh, A., 2011, Focal mechanism determination using relative moment tensor inversion for some earthquakes in Zarand (Iran): MSc. Thesis, University of Tehran, Institute of Geophysics, Tehran, Iran.

Sakaguchi, K., and Yokoyama, T., 2017, Changes in in-situ rock stress before and after the major 2011 Tohoku-Oki earthquake: Procedia Engineering, **191**, 768-775, doi:10.1016/j.proeng.2017.05.243.

Shebalin, P., and Narteau, C., 2017, Depth dependent stress revealed by aftershocks: Nature Communications, **8**(1), doi:10.1038/s41467-017-01446-y.

Shevell, S. K., 2003, The Science of Color: Amazon, Elsevier, www.amazon.com/Science-Color-Steven-K-Shevell/dp/0444540202.

Stewart, S. A., Harvey, M. J., Otto, S. C., and Weston, P. J., 1996, Influence of salt on fault Geometry: Examples from the UK Salt basins: Geological Society, London, Special Publications, **100**(1), 175-202, doi:10.1144/gsl.sp.1996.100.01.12.

Talebian, M., and Jackson, J., 2004, A reappraisal of earthquake focal mechanisms and active shortening in the Zagros mountains of Iran: Geophys. J. I., **156**, 506–526.

Tatar, M., Hatzfeld, D., and Ghafory-Ashtiany, M., 2004, Tectonics of the Central Zagros (Iran) deduced from microearthquake seismicity: Geophys. J. I., **156**, 255–266.

Wallace, R. E., 1951, Geometry of shearing stress and relation to faulting: Journal of Geology, **59**, 111-130.

Wang, C., Song, C., Guo, Q., Mao, J., and Zhang, Y., 2015, New insights into stress changes before and after the Wenchuan earthquake using hydraulic fracturing measurements: Engineering Geology, 194, 98-113, doi:10.1016/j.enggeo.2015.05.016.

Yaminifard, F., Hatzfeld, D., Farahbod, A. M., and Mokhtari, M., 2007, The diffuse transition between the Zagros continental collision and the Makran oceanic subduction (Iran): microearthquake seismicity and crustal structure: Geophys. J. I., **170**, 182–194.

Yaminifard, F., Sedghi, M. H., Gholamzadeh, A., Tatar, M., and Hessami, K., 2012, Active faulting of the southeastern-most Zagros (Iran): Microearthquake seismicity and crustal structure: Journal of Geodynamics, **55**, 56-65, doi:10.1016/j.jog.2012.01.003.

Zoback, M. L., 1992, First and second-order patterns of stress in the lithosphere: The world stress map project: J. Geophys. Res., **97**, 11703-11728, doi 10.1029/92jb00132.